Quasi-Stationary Zonally Asymmetric Circulations in the Equatorial Lower Mesosphere

MATTHEW H. HITCHMAN* AND CONWAY B. LEOVY

Department of Atmospheric Sciences, University of Washington, Seattle, WA 98195

JOHN C. GILLE AND PAUL L. BAILEY

National Center for Atmospheric Research, Boulder, CO 80307

(Manuscript received 19 May 1986, in final form 12 February 1987)

ABSTRACT

Data from the Limb Infrared Monitor of the Stratosphere (LIMS) are used to identify a new type of planetary scale disturbance in the equatorial lower mesosphere during northern winter 1978/79. The disturbances consist of two or three vertically stacked temperature extrema of alternating sign. They persist for as long as two weeks and do not propagate. Their occurrence is confined to regions of very weak or negative inertial stability, and their meridional to vertical aspect ratio, meridional structure and zonal spectrum are consistent with disturbances predicted by inertial instability theory. However, they are found only when there is strong forcing of the subtropical mesosphere by zonal wavenumber one and two Rossby waves. This fact, together with the absence of zonal propagation, suggests that stationary Rossby waves determine their occurrence and longitudinal structure. These structures can significantly modify the zonal mean flow and should be taken into account in dynamical models of the equatorial mesosphere.

1. Introduction

The Limb Infrared Monitor of the Stratosphere (LIMS) on the Nimbus 7 satellite sampled the middle atmospheric large-scale temperature structure over most of the planet with high vertical resolution during the period October 1978–May 1979 (Gille and Russell, 1984). Zonal mean distributions of temperature, zonal wind, and residual circulation have been previously described (Hitchman and Leovy, 1986; hereafter HL) and the dominant time variations were attributed to the semiannual oscillation (SAO). Much of the planetary wave signal in LIMS data at low latitudes is due to downward and eastward phase propagation of Kelvin waves and to quasi-stationary Rossby waves of midlatitude origin, but a third type of temperature disturbance was sometimes present in the lower mesosphere. This paper describes and discusses this previously unrecognized phenomenon.

Figure 1 shows the time-height variations of the mapped wavenumber 1 and 2 cosine coefficients of temperature over equatorial latitudes for the first 87 days of the LIMS record. Kelvin waves, previously identified in LIMS data by Salby et al. (1984) and Coy and Hitchman (1984), appear as alternating positive and negative features sloping downward with time. Amplitude extrema for these waves are marked with "H" and "L". Some of the signals in Fig. 1 are also due to Rossby waves propagating from midlatitudes. These can be identified from their signatures in latitude–height and latitude–longitude sections. The strong thermal disturbances in the boxes marked A, B, and C in Fig. 1 fall in neither class. They are characterized by the presence of two or three vertically stacked temperature extrema. Their amplitudes are large, generally exceeding the amplitudes of the Kelvin waves. They are confined to low latitudes, predominantly in the Northern (winter) Hemisphere, and they show no evidence for propagation in altitude or latitude, and little or no evidence for propagation in longitude. Unlike Kelvin and Rossby waves, for which separate wavenumber 1 and 2 events are the rule, these disturbances are characterized by simultaneous amplification of the lowest two or three wavenumber components of the temperature field. They develop rapidly, and persist as stationary disturbances for one or two weeks, extending beyond the time boundaries of the boxes in Fig. 1. These boxes delineate cases which will be discussed in detail to demonstrate the characteristics just described.

Following a description of the data and analysis (section 2), we discuss the structure of the disturbances, validate the disturbance signatures in LIMS data by comparison with rocket soundings, and discuss their inferred wind and vertical velocity fields (section 3). Signatures of these disturbances are observed only when the LIMS data show that two conditions are satisfied: the region in which they occur is inertially unstable in the zonal mean, and there is strong forcing of the equa-

* Present affiliation: National Center for Atmospheric Research, Boulder, CO, 80307.

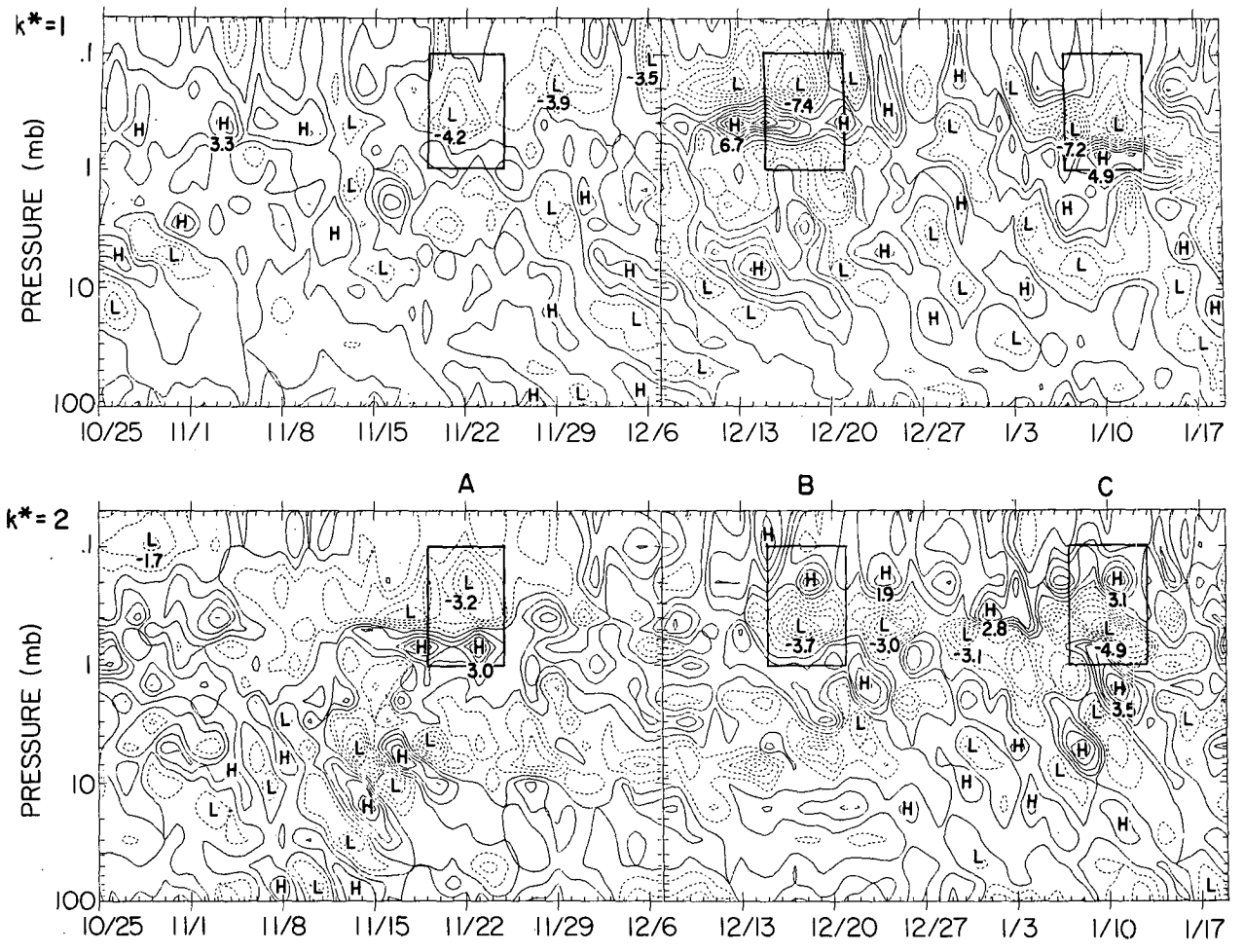

FIG. 1. Time–height section of LIMS temperature cosine coefficient for wave 1 (upper, contour interval 1 K) and wave 2 (lower, contour interval 0.5 K), averaged in the latitude band 8°S–8°N, for the period 25 October 1978–19 January 1979. Cases A, B and C center on 22 November, 18 December and 10 January. H and L groups denote Kelvin wave packets.

torial mesosphere by Rossby waves propagating from the winter hemisphere (sections 4 and 5).

The disturbance characteristics and conditions of formation suggest that inertial instability is essential for their formation. A comparison of the observations with some results from inertial instability theory is given in section 6, together with a brief discussion of the possible role of these disturbances in modifying the zonal mean flow. To avoid attaching a label which implies that we are sure of their origin, we refer to them simply as *pancake structures.*

2. Data and analysis

a. Temperature

LIMS temperatures are available in the form of mapped synoptic coefficients at 1200 UTC during the period 25 October 1978–28 May 1979. Thirteen zonal harmonic coefficients (the zonal mean plus the cosine and sine coefficients of the first six zonal wavenumbers) are provided at 4 degree intervals from 64°S to 84°N and at 18 standard pressure levels ranging from 100 to 0.05 mb (~16–70 km), with a spacing of ~3.2 km. Temperatures derived from the inversion algorithm of Bailey and Gille (1986) are used.

Detection of coherent zonally asymmetric phenomena with short vertical wavelengths depends on the precision and vertical resolution of the retrieved temperatures. In the lower mesosphere the precision is ~0.5 K (Gille et al., 1984). The effective vertical resolution of individual profiles is ~2 km. In the region crucial to this study, temperatures are mapped at 1.0, 0.7, 0.5, 0.4, 0.2, 0.1 and 0.05 mb. The effective Nyquist wavelength is ~6.4 km for the lower mesosphere. Features with amplitudes larger than 2 K and vertical wavelengths larger than 7 km should be represented in this dataset. Kelvin waves with vertical wavelength ~10 km are readily resolved by mapped LIMS temperature fields (Salby et al., 1984). However, pancake structures have not been described previously. To establish the reality of these structures, we rely on their

spatial and temporal coherence, verification by rocket profiles, and similarity with theoretical expectations. Rocketsonde temperature values at LIMS standard pressure levels are used for comparison with mapped LIMS fields interpolated to rocket station locations (cf. HL).

b. Geostrophic and balance eddy winds

Hitchman and Leovy describes construction of geopotential height fields from National Meteorological Center (NMC) 50 mb heights and LIMS temperatures, and calculation of zonal mean gradient zonal winds. Reasonable estimates of eddy horizontal winds from imperfect geopotential height field data are difficult to make in the tropics. A modified geostrophic approximation for the zonal and meridional eddy components consistent with the zonal mean gradient zonal wind is

$$u'_g = -\frac{1}{\gamma}\frac{\partial \Phi'}{\partial y}, \quad v'_g = \frac{ik\Phi'}{f + \bar{u}\tan\phi/a}, \tag{2.1}$$

where u'_g, v'_g, and Φ' are velocity component and geopotential amplitudes, with i indicating a 90° phase lead of v'_g relative to Φ'; $\gamma = f + 2\bar{u}\tan\phi/a, f = 2\Omega\sin\phi$; k is zonal wavenumber; ϕ is latitude; a is the Earth's radius, and Ω is rotation frequency. Although differing by the term $\bar{u}\tan\phi/a$, we refer to these winds as geostrophic winds.

Approaching the equator, certain advection terms can become comparable to, or larger than, the Coriolis terms in the momentum equations. Neglecting eddy flux terms and advection by the mean meridional circulations as small (Andrews and McIntyre, 1976), we write the horizontal momentum equations as

$$\left.\begin{aligned} \frac{\partial u'}{\partial t} + \bar{u}\frac{\partial u'}{\partial x} - \eta v' &= \frac{-\partial \Phi'}{\partial x} + f'_x \\ \frac{\partial v'}{\partial t} + \bar{u}\frac{\partial v'}{\partial x} + \gamma u' &= \frac{-\partial \Phi'}{\partial y} + f'_y \end{aligned}\right\}, \tag{2.2}$$

where

$$\eta = f - \frac{1}{\cos\phi}\frac{\partial}{\partial y}(\cos\phi\,\bar{u})$$

is the absolute vorticity of the zonal mean flow. An analytic solution to (2.2) may be obtained if each zonal wave has the form $e^{i(kx-\omega t)}$, where ω = frequency, and if Rayleigh friction is assumed: $(f'_x, f'_y) = (-\mu u', -\mu v')$. The solution is

$$\left.\begin{aligned} u' &= \left\{-\eta\frac{\partial \Phi'}{\partial y} - ik\Phi'(\mu + ik\left[\bar{u} - c_x\right]\right\}\Big/ D^* \\ v' &= ik\left[\gamma\Phi' - \left(\bar{u} - c_x - \frac{i\mu}{k}\right)\frac{\partial \Phi'}{\partial y}\right]\Big/ D^* \end{aligned}\right\}, \tag{2.3}$$

where

$$D^* = \eta\gamma + [\mu + ik(\bar{u} - c_x)]^2 \quad \text{and} \quad c_x = \omega/k.$$

The pancake structures and the predominant Rossby waves are quasi-stationary. Kelvin waves have high values of c_x, but because they consist of vertically oscillating temperature perturbations of much smaller amplitude than pancake structures and Rossby waves, their contribution to height fields is relatively small. Consequently, we neglect c_x in (2.3). Because its magnitude is unknown, we also neglect friction, except as described below. The resulting solution, hereafter referred to as balance winds, is

$$\left.\begin{aligned} u'_b &= -\left(\eta\frac{\partial \Phi'}{\partial y} - k^2\bar{u}\Phi'\right)\Big/ D \\ v'_b &= ik\left(\gamma\Phi' - \bar{u}\frac{\partial \Phi'}{\partial y}\right)\Big/ D \end{aligned}\right\}, \tag{2.4}$$

where $D = \eta\gamma - (k\bar{u})^2$. With the exception of a few locations, $D \approx f(f - \partial\bar{u}/\partial y)$ and

$$\left.\begin{aligned} \frac{u'_b}{u'_g} &\approx \left(1 - \frac{k^2\bar{u}\Phi'}{\eta\partial\Phi'/\partial y}\right) \\ \frac{v'_b}{v'_g} &\approx \frac{f}{\eta}\left(1 - \frac{\bar{u}\partial\Phi'/\partial y}{f\Phi'}\right) \end{aligned}\right\}. \tag{2.5}$$

This form displays more clearly than (2.4) the roles of the two important processes that are represented in the balance winds but not the geostrophic winds: zonal advection of eddy winds ($\bar{u}\partial u'/\partial x$, $\bar{u}\partial v'/\partial x$), represented by the second terms in parentheses in (2.5), and eddy advection of the zonal mean wind, whose effect enters through the factor η. If the meridional shear of zonal mean wind is so large that $f(f - \partial\bar{u}/\partial y) \approx f\eta \approx D < 0$, the region is inertially unstable, and the sign of v'_b is usually opposite to that of v'_g.

The geostrophic wind is singular at the equator. In (2.1) this is removed by setting the equatorial values to the mean of values at 4°S and 4°N. For the balance winds, this singularity splits into two at the latitudes where $f \approx \frac{1}{2}\{\bar{u}_y \pm [\bar{u}_y^2 + (2k\bar{u})^2]^{1/2}\}$. For small zonal advection, these singularities occur near the boundaries of the inertially unstable zone, at the latitudes where $f \approx 0$ and $f \approx \bar{u}_y$. As zonal advection increases, these singular latitudes move farther apart. Singularities in balance winds are removed by introducing friction as in (2.3) with the value $\mu_0 = 1\ \text{day}^{-1}$. If $D = 0$ at a grid point, we set $D = \mu_0^2$. If $0 < |D| < \mu_0^2$, we substitute $D = |D|^{-1}D\mu_0^2$ to preserve sign. At all other points, friction is omitted. The chosen value of μ_0 is such that $\mu_0 < |f|$ at latitudes greater than 5°.

The observed temperature fields in the tropics have rather low signal to noise for wind field estimates. Consequently we have modified the balance winds (2.4) in three further ways. Because $\bar{u}_y$ varies rapidly in latitude, the data sometimes indicate two inertially unstable zones in the 4°S–24°N region. From (2.5), four reversals of v'_b would be expected in such a region. Such rapidly oscillating behavior is unrealistic, and to avoid it we have smoothed $\bar{u}_y$, for use in (2.4) only, with a

¼–½–¼ filter. The result is at most a single broader region of negative η in (2.4) and only two corresponding wind reversals. The second modification is based on observational and modeling studies of equatorial winds in the planetary boundary layer which show that the height gradient term always dominates the advection terms (Krishnamurti and Wong, 1979; Reverdin and Sommeria, 1983; Stout and Young, 1983; van Tuyl, 1986). We have chosen to impose this behavior on our solutions. A measure of the relative magnitudes of the zonal advection and height gradient terms in (2.2) is

$$A = \frac{(k\bar{u})^2(u'^2 + v'^2)}{(k\Phi')^2 + (\partial\Phi'/\partial y)^2}.$$

At each latitude and for each wavenumber, if $A > 0.9$ initially, eddy wind coefficients are reduced by the factor $[0.8/(A + 0.1)]^{1/2}$, so that A is forced to be slightly less than unity. Since zonal mean wind and height fields vary fairly smoothly, this change does not introduce abrupt variations in u'_b and v'_b. Modest reductions are effected in strong zonal flow where D is also small. Finally, all balance and geostrophic eddy wind components are smoothed ¼–½–¼ in latitude.

This approach produces at best only a crude approximation to the true winds in the deep tropics, but it has certain advantages. In contrast to the geostrophic solution, for which the meridional components reverse sign across the equator, this approach yields smoothly varying eddy winds. Unlike the usual balance equation expressed in terms of a streamfunction (Shuman, 1957), eddy winds are readily obtainable in regions of inertial instability, and the assumption that the winds are nondivergent is not imposed. Direct comparison of eddy winds with rocketsonde eddy winds is difficult because tides and gravity waves are important components affecting the rocket winds, especially at low latitudes. The limited comparisons that we have made indicate that the balance winds agree slightly better with rocketsondes than do geostrophic winds. For these reasons, we believe that the derived balance winds give a qualitatively correct, though quantitatively crude, depiction of the true slowly varying eddy wind field in low latitudes.

c. *Eliassen–Palm fluxes*

Balance eddy winds are used to calculate Eliassen–Palm fluxes due to quasi-stationary waves. For a discussion of the relative utility of using balance over geostrophic winds in calculating this flux, see Robinson (1986).

The transformed Eulerian mean zonal momentum equation is

$$\frac{\partial\bar{u}}{\partial t} - \eta\bar{v}_* + \frac{\partial\bar{u}}{\partial z}\bar{w}_* = \frac{1}{\rho_0 a\cos\phi}\nabla\cdot\mathbf{F}, \qquad (2.6)$$

where $\bar{v}_*$ and $\bar{w}_*$ are the meridional and vertical components of the residual mean circulation, and

$$\nabla\cdot\mathbf{F} = \frac{1}{\cos\phi}\frac{\partial}{\partial y}(\cos\phi F_{(y)}) + \frac{\partial}{\partial z}(F_{(z)}). \qquad (2.7)$$

The components of the Eliassen–Palm flux $\mathbf{F}$ are given by

$$\left.\begin{aligned} F_{(y)} &= \rho_0 a\cos\phi\left[\frac{\partial\bar{u}/\partial z}{\partial\bar{\theta}/\partial z}\cdot\overline{v'\theta'} - \overline{u'v'}\right] \\ F_{(z)} &= \rho_0 a\cos\phi\left[\frac{\eta}{\partial\bar{\theta}/\partial z}\cdot\overline{v'\theta'} - \overline{u'w'}\right] \end{aligned}\right\}, \qquad (2.8)$$

where θ is potential temperature and ρ_0 is basic state density (Andrews and McIntyre, 1976; Boyd, 1976). In (2.8), both terms in $F_{(y)}$ are computed from the balance winds.

At most locations the heat flux term is less than 10%, and is at most ~50%, of the momentum flux term in $F_{(y)}$. The term $\overline{u'w'}$ is omitted in $F_{(z)}$ because of its expected small relative size and the additional difficulties involved in its calculation. A qualitative assessment of its role in some situations is given in section 6c, however. With the $\overline{v'\theta'}$ term omitted in $F_{(y)}$, and $\overline{u'w'}$ omitted in $F_{(z)}$, the components of $\mathbf{F}$ correspond to the quasi-geostrophic approximation, except for differences between η and f. Note that small values of η imply small values of $F_{(z)}$. The distribution of $\mathbf{F}$ is given in section 5 in the form of vector plots in the meridional plane with components $F_{(y)}/\rho_0$ and $138F_{(z)}/\rho_0$.

3. Properties of tropical planetary scale disturbances

a. *Kelvin waves, Rossby waves, and pancake structures*

Most of the features in Fig. 1 can be ascribed to Kelvin waves, Rossby waves, or pancake structures. The differences among these are illustrated for cases A, B and C in Figs. 2–5. Zonal mean zonal winds in which they occur are shown in Fig. 6.

The vertical and zonal wavelengths and period for each diagonally sloping feature marked "H" or "L" in Fig. 1 are consistent with the dispersion relation governing the behavior of 2-D internal gravity waves, of which the equatorially trapped atmospheric Kelvin wave is a special kind (Coy and Hitchman, 1984). In equatorial longitude–height sections for cases B and C, Kelvin waves appear as eastward sloping wave 1 temperature anomalies between 10 and 0.7 mb (Fig. 2, left).

Rossby waves reaching the subtropics appear as westward sloping temperature waves. For example, on 18 December 1978 (case B), there is a strong westward sloping wave 1 feature with vertical wavelength $L_z \sim 45$ km in the 24°–32°N latitude band, and on 10 January 1979 (case C), there is a westward-sloping wave 2 feature with vertical wavelength ~ 75 km (Fig. 2, right). For case A (22 November 1978), a less coherent Rossby wave feature can be seen. Rossby waves sometimes penetrate to the equator. An example is the westward-sloping equatorial feature on 18 December indicated

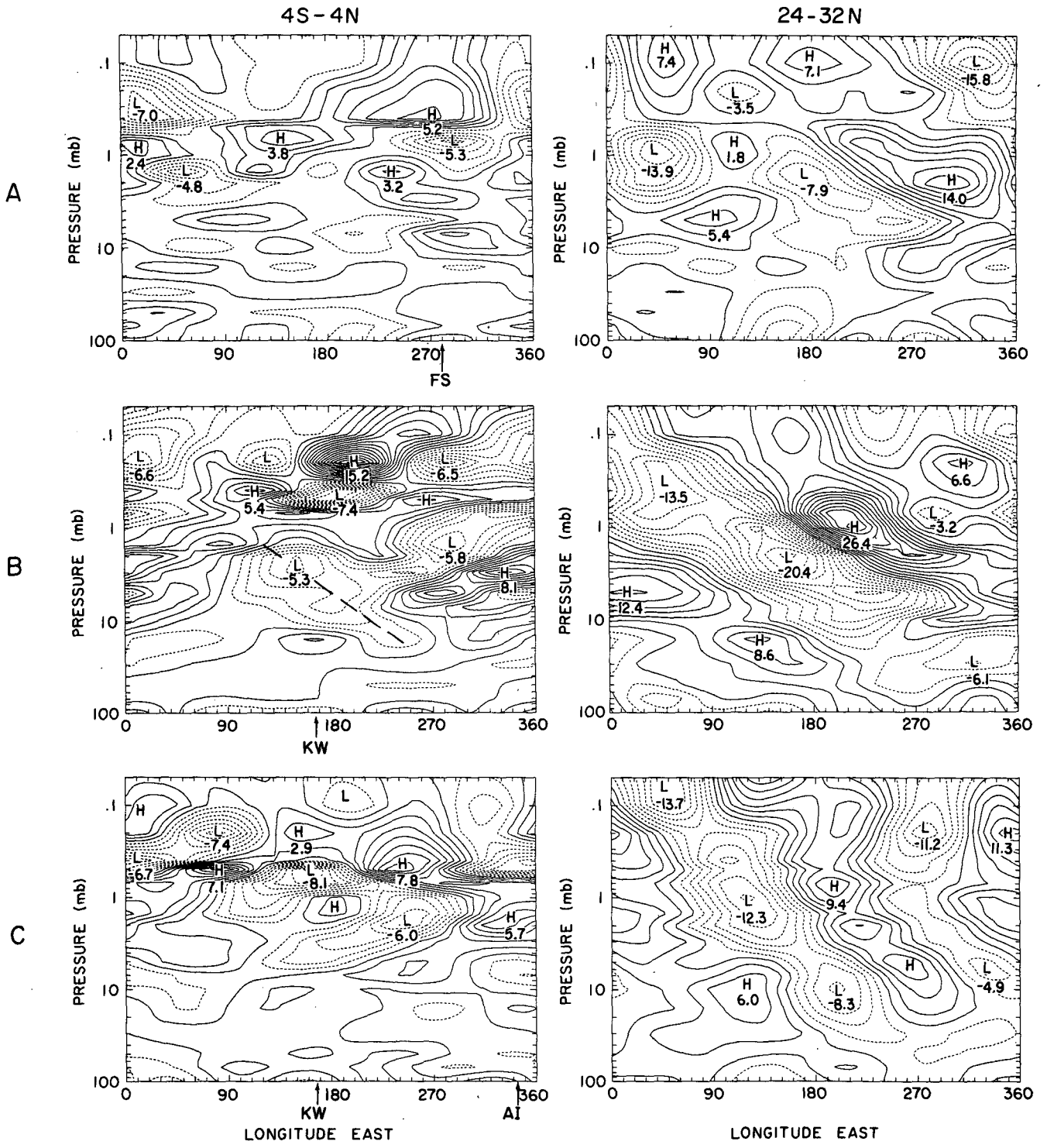

FIG. 2. Longitude–height sections of LIMS temperature averaged in the latitude bands 4°S–4°N (left, contour interval 1 K) and 24°–32°N (right, contour interval 2 K) on 22 November 1978, 18 December 1978 and 10 January 1979 (cases A, B and C). Zonal waves 1, 2, and 3 are included in the analysis. Arrows indicate the longitudes of Kwajalein (KW; 8.7°N, 167.7°E), Fort Sherman (FS; 9.3°N, 280.0°E), and Ascension Island (AI; 8.0°S, 14.4°W).

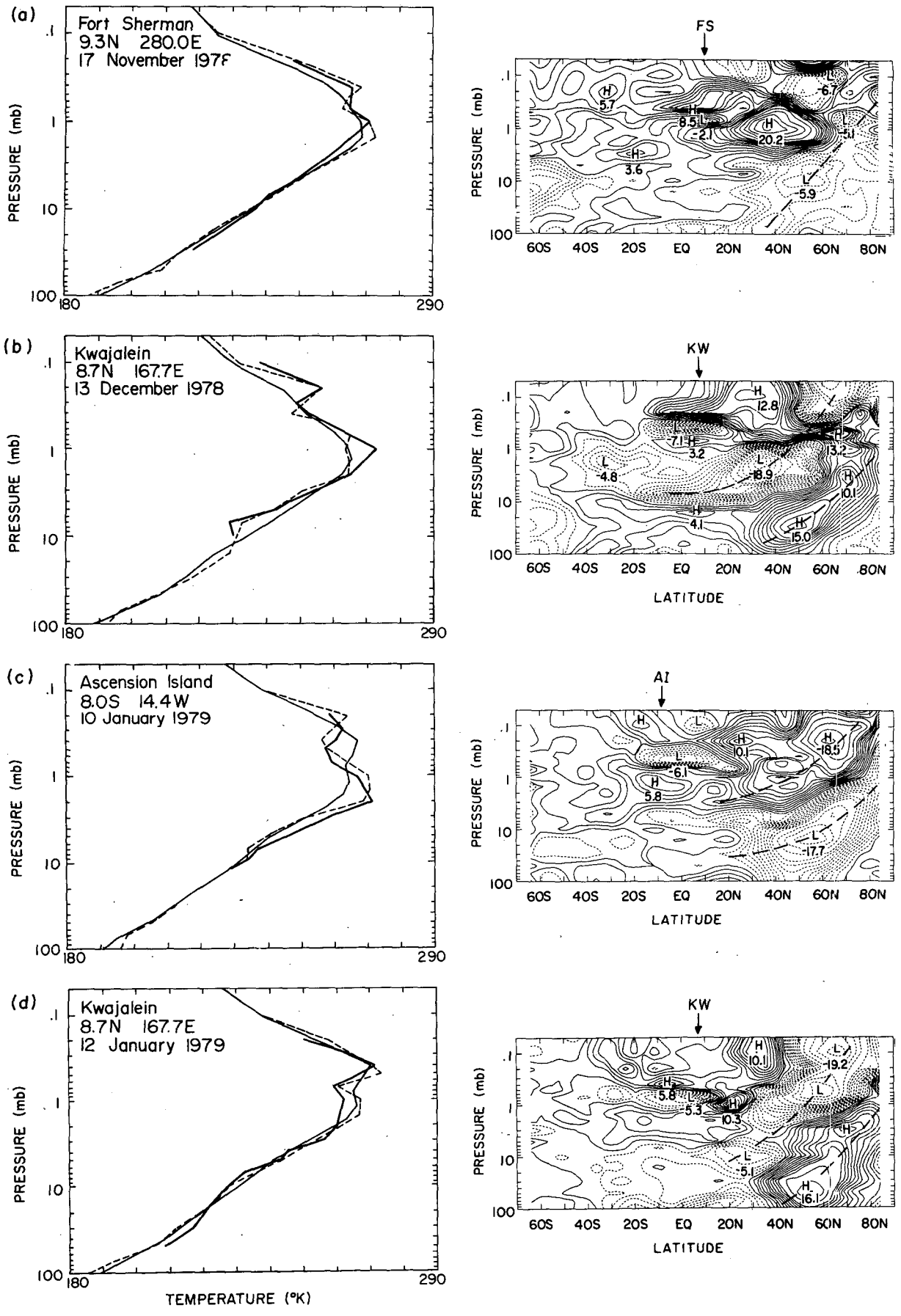
(a)
Fort Sherman
9.3N 280.0E
17 November 1978
PRESSURE (mb)
.1
1
10
100
180
290
FS
H
5.7
L
-6.7
H
8.5
L
-2.1
H
20.2
L
-5.1
H
3.6
L
-5.9
60S 40S 20S EQ 20N 40N 60N 80N
(b)
Kwajalein
8.7N 167.7E
13 December 1978
KW
H
12.8
L
-7.1
H
3.2
H
13.2
L
-4.8
L
-18.9
H
10.1
H
4.1
H
15.0
LATITUDE
(c)
Ascension Island
8.0S 14.4W
10 January 1979
AI
H
H
10.1
H
18.5
L
-6.1
H
5.8
L
-17.7
(d)
Kwajalein
8.7N 167.7E
12 January 1979
KW
H
10.1
L
-19.2
H
5.8
H
5.3
H
10.3
L
-5.1
H
16.1
TEMPERATURE (°K)

by the dashed line in Fig. 2B. It is coherent with the Rossby wave at high latitudes. Rossby waves have slopes that are upward and westward, upward and poleward, and poleward and eastward. The signature of Rossby waves in the latitude–height plane at fixed longitude is illustrated in Fig. 3. The characteristic poleward and upward sloping axes of maximum temperature anomaly are marked by dashed curves. Note the penetration of Rossby waves to the equatorial stratosphere during December and January.

Pancake structures shown in Figs. 2 and 3 are vertically stacked with no slopes to their phase surfaces in either latitude or longitude. Temperature perturbation amplitudes are large, generally exceeding 5 K, and they are confined to the equatorial mesosphere. Although they occur when Rossby waves are active, they are readily distinguished from Rossby waves because of their equatorial confinement, lack of phase tilt, and small vertical scale. Their longitudinal structure is not dominated by a single zonal wavenumber component; wavenumbers 1–3 all contribute to the structures shown in Fig. 2 (cf. Fig. 7). Pancake structures show a characteristic relationship to the zonal mean wind. They are centered between 0.4 and 0.7 mb, with their locus of activity gradually descending with time following an incursion of easterly mean zonal winds into the winter hemisphere (compare the right-hand panels of Fig. 3 and Fig. 6).

b. *Validation*

Available rocket soundings were thoroughly examined for validation of pancake structures. Rocket station locations and launch times were such that they usually did not coincide with maximum temperature amplitudes. Only four suitable soundings were found. These are compared with LIMS soundings in Fig. 3. The quasi-stationarity of the pancake structures allows comparison of Fig. 3a with case A, Fig. 3b with case B, and Figs. 3c, d with case C in Fig. 1. The LIMS temperature structure in the meridional plane at the appropriate station longitude and time is also provided in Fig. 3.

In each comparison, the rocket and corresponding LIMS profile show similar large temperature excursions in the lower mesosphere. Agreement between the rocket soundings and LIMS profiles is generally excellent, but the zonal mean LIMS sounding for the same latitude is quite different from the local sounding. LIMS picks up both the location and intensity of the zonally asymmetric features measured by the rockets, and the signature of pancake structures in individual rocket temperature soundings is the prominent double stratopause. The descent of the zonal mean warm westerlies of the semiannual oscillation (SAO) also produces a double stratopause, but it is weaker, as shown by the zonal mean LIMS temperature profiles for case C (Figs. 3c, d; see also HL).

c. *Horizontal winds and vertical velocities*

Temperature distributions in the longitude–latitude plane at levels corresponding to overlying warm and cold anomalies are shown in Fig. 4 for cases A, B and C. Note the equatorial confinement of the temperature anomalies, the absence of phase shift with latitude, and the reversal of the equatorial temperature anomaly between levels. North of latitude 20°–30°N, the temperature anomalies tend to shift eastward with latitude and westward with height. There is a definite phase shift between these Rossby wave structures and the pancake structures, especially in cases B and C.

Figure 5 shows geopotential height fields for each of these cases. The levels shown lie between overlying equatorial temperature extrema of opposite sign in cases A and C and near the top of a cold anomaly centered near 0°N, 170°E in case B. Note the correspondence in sign between the height anomalies and the underlying temperature anomaly. Both balance and geostrophic winds are shown. The meridional component of the balance wind tends to be larger but varies more smoothly with latitude than the geostrophic wind in the latitude band 5°S–25°N.

The geopotential anomalies associated with pancake structures lie in a belt of weak zonal mean winds between the strong summer easterlies and winter westerlies. This belt gradually shifts northward from 15°S–15°N in November to 0°–25°N in January. Significant height anomalies are centered close to the equator and slope westward with latitude in the northern hemisphere. The corresponding balance wind fields exhibit longitudinally localized bands of strong meridional flow, for example: strong southeastward flow from 25°N to the equator near 90°E at 0.4 mb on 18 December, and strong northwestward flow from the equator to 25°N near 270°E at 0.7 mb on 10 January. This flow configuration is consistent with equatorward momentum fluxes or poleward EP fluxes.

The equatorial temperature extrema associated with the pancake structures are due to vertical motions. Because of the long time scale, the vertical velocity can be estimated by balancing the vertical motion and ra-

FIG. 3. A comparison of LIMS and rocket temperature profiles at rocket station locations (left) at (a) Fort Sherman on 17 November 1978, (b) Kwajalein on 13 December 1978, (c) Ascension Island on 10 January 1979, and (d) Kwajalein on 12 January 1979, together with latitude–height sections of LIMS temperature for waves 1–3 at the corresponding longitude and date (right). At left the rocket profile is the heavy solid line; the light solid line is LIMS zonal mean only; and the dashed line is LIMS zonal mean plus waves 1–6. At right, the heavy dashed lines indicate Rossby wave phase axes. The contour interval is 1 K between −12 K and +12 K and 2 K for larger values. Values have been smoothed ¼–½–¼ in latitude.

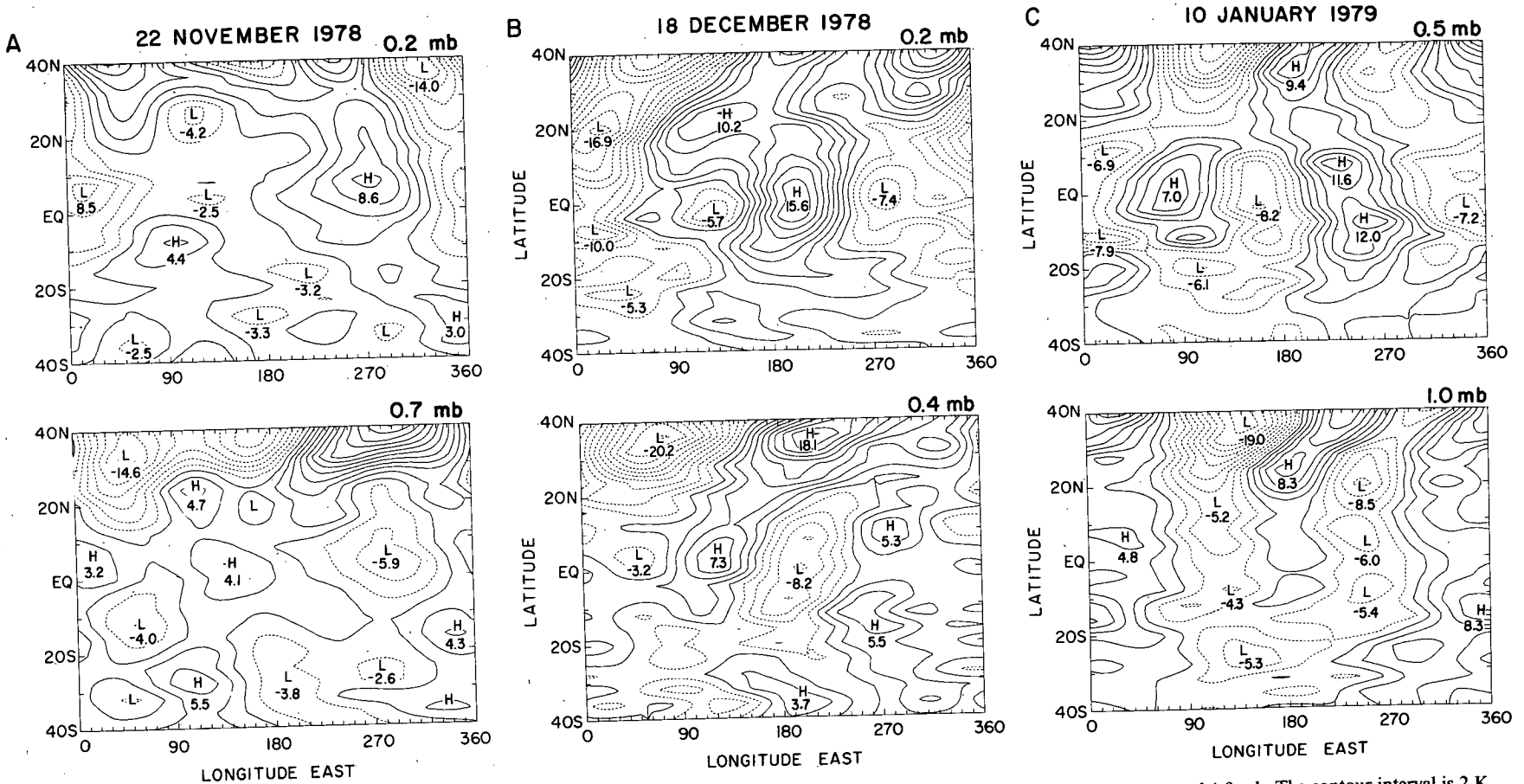

FIG. 4. Plan views of LIMS temperature waves 1–3 for case A (left) at 0.2 and 0.7 mb, case B (middle) at 0.2 and 0.4 mb, and case C (right) at 0.5 and 1.0 mb. The contour interval is 2 K.

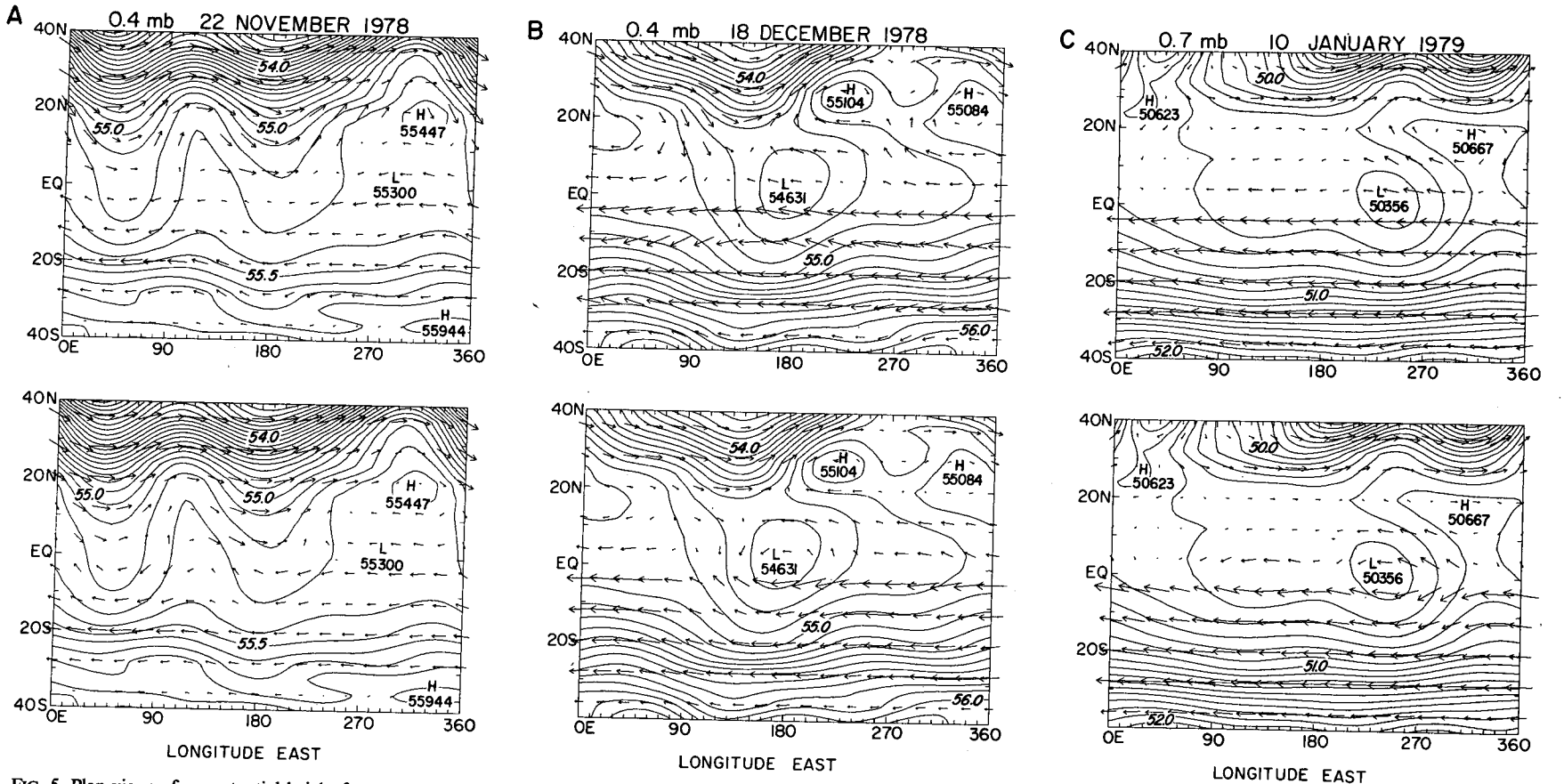

FIG. 5. Plan views of geopotential height for case A at 0.4 mb (left), case B at 0.4 mb (middle) and case C at 0.7 mb (right), comparing balance (upper) and geostrophic (lower) winds. The contour interval is 100 m. Waves 1–3 are included, plus the zonal mean for the zonal component. Vectors point in the azimuthal direction toward which the air is moving. Reference speeds in case B at (0°E, 4°S) are $u_g = -98$, $v_g = -21$, $u_b = -87$, $v_b = -1$ m s^{-1}.

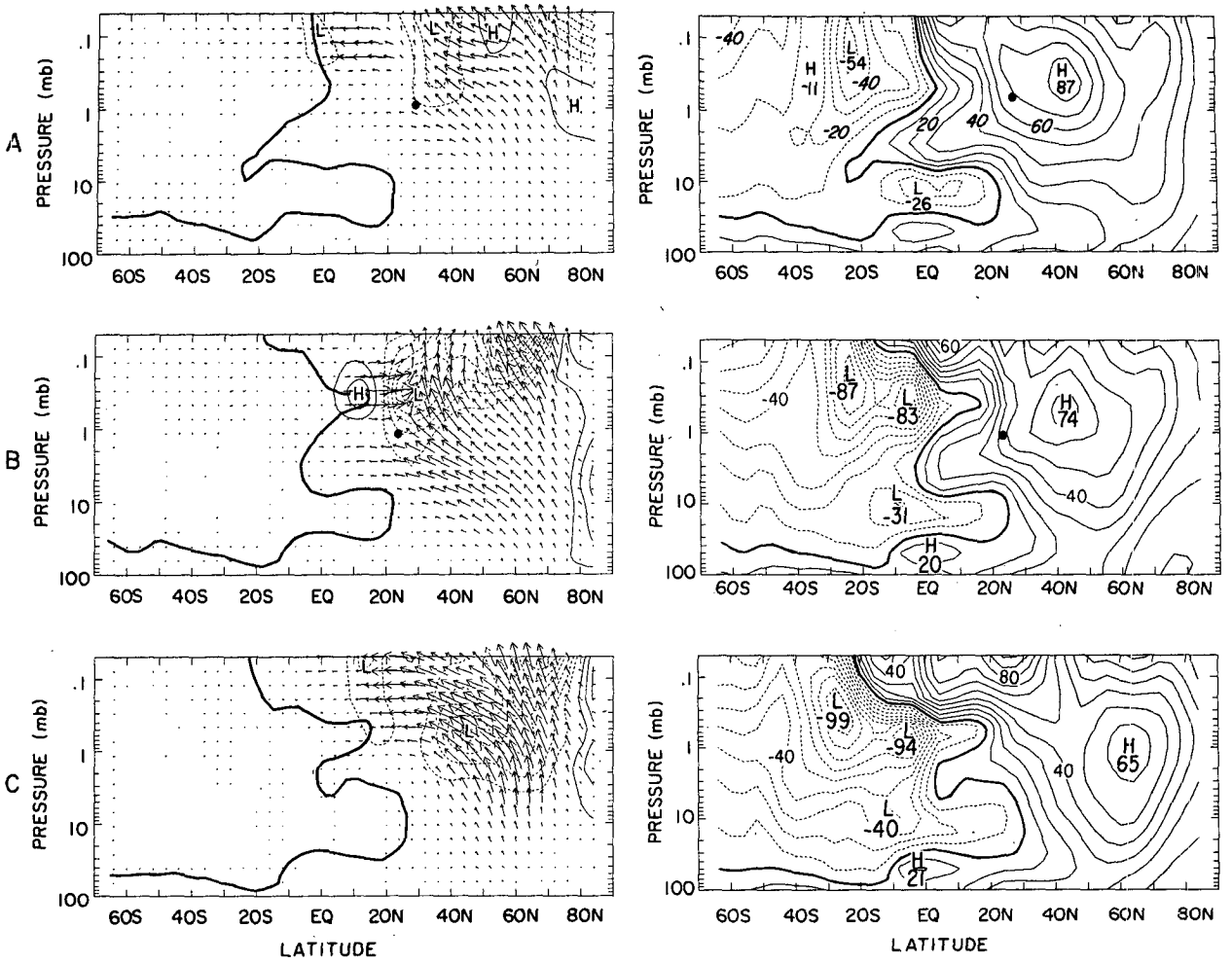

FIG. 6. Latitude–height sections of six-day average EP fluxes and their divergences, summed for waves 1 and 2 (left) and of zonal mean zonal wind (right), for the periods 18–23 November 1978 (A), 12–17 December 1978 (B), and 5–10 January 1979 (C). Contour intervals are 5 m s^{-1}/day (left) and 10 m s^{-1} (right). Balance eddy winds are used in EP flux calculations (see text). The zero contour of EP flux divergence has been removed for clarity. The zero wind line has been traced onto each EP flux section. The large dot in A and B indicates a region of splitting of wave action flux (see text).

diative damping terms in the thermodynamic energy equation. This gives $|w'| \sim |\bar{T}'| \cdot g/(\bar{T}\tau N^2)$ where τ is the radiative damping time scale. Taking $\tau \sim 2$ days (Fels, 1982, 1984), $|T'| \sim 10$ K, $g \sim 10$ m s^{-2}, $T \sim 250$ K, and $N \sim 0.02$ s^{-1}, the layered structures over the equator can be maintained by $|w'| \sim 0.5$ cm s^{-1}. The corresponding divergent part of the horizontal wind can be estimated from the continuity equation. The vertical scale (half-wavelength) of the temperature anomalies is ~7 km, and the meridional scale is ~2500 km (25° latitude). The ratio of meridional to vertical scales is $\delta \sim 360$, and the divergent meridional wind is $v'_\delta \sim \delta \cdot |w'| \sim 2$ m s^{-1}. This is too small to appear above the noise of the balance wind analysis shown in Fig. 5. Nevertheless, the strong meridional balance wind flow patterns in cases B and C in Fig. 5 are consistent with the schematic vertical eddy circulation pattern shown in Fig. 8. We suggest that the sinking motion in equatorial warm anomalies and rising motion in cool anomalies is completed by meridional flow between the warm and cool anomalies and by compensating sinking and rising motion near 25°N, near the equatorward edge of the Rossby wave regime.

4. Relationship between pancake structures and inertial instability

A time-height section of the quantity

$$\tilde{P} = \begin{cases} |f| \cdot \left[1 - \dfrac{1}{\mathrm{Ri}} - \dfrac{\bar{u}_y}{f}\right], & y \neq 0 \\ 0, & y = 0, \end{cases} \tag{4.1}$$

where $\mathrm{Ri} = N^2/(\bar{u}_z)^2$, is shown in Fig. 9. $\tilde{P}$ is closely related to both the zonal mean Ertel potential vorticity and the isentropic gradient of angular momentum (cf.

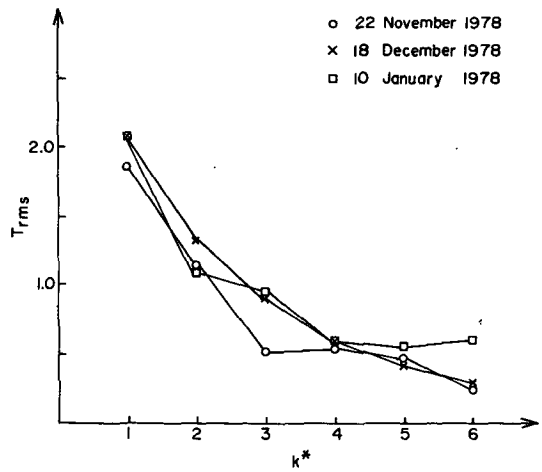

FIG. 7. The variation of zonal rms temperature with nondimensional zonal wavenumber, averaged over 8°S–8°N and over the rectangular regions in Fig. 1 for cases A (circles), B (crosses), and C (squares).

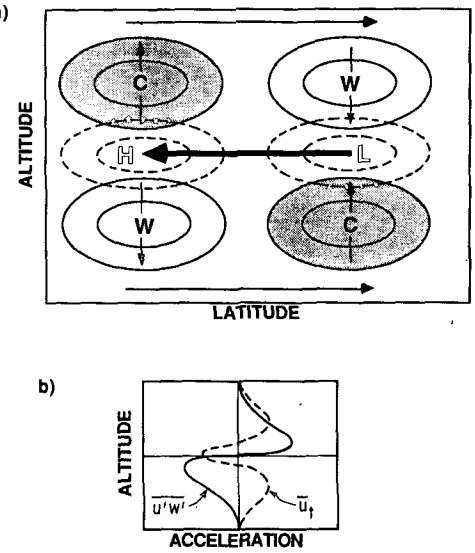

FIG. 8. (a) Schematic view of hypothesized pancake structure in the meridional plane [isotherms (solid), cold (shaded), geopotential (dashed)]. The vertical branches on the northern edge merge with Rossby waves and slope in and out of the plane of the figure. The meridional branch curves in and out of the plane around geopotential high and low centers, as in Fig. 5b, c. (b) Schematic depiction of vertical eddy momentum flux and momentum flux divergence (see section 6c).

HL); $\tilde{P} < 0$ only if $\bar{u}_y/f > (1 - \mathrm{Ri}^{-1})$. This exceptional condition is the necessary condition for inviscid inertial instability (Eliassen and Kleinschmidt, 1957), and it will be referred to as anomalous $\tilde{P}$. In inviscid theory, whenever $\tilde{P} < 0$, meridionally displaced parcels will accelerate. Normally the term Ri^{-1} in $\tilde{P}$, which arises from isentropic slopes, is negligible.

Regions of anomalous $\tilde{P}$ are almost entirely due to strong meridional shear and only occur within ~25° of the equator, predominantly in the winter hemisphere (HL). The occurrence of anomalous $\tilde{P}$ in the band 4°–12°N (Fig. 9) coincides closely with that of pancake structures (compare Figs. 1 and 9). The level of anomalous $\tilde{P}$ descends with time along with the pancake structures. However, during the November–January period of continuously anomalous $\tilde{P}$, pancake structures are not observed unless Rossby waves are nearby. We found no pancake structures in regions of anomalous $\tilde{P}$ in February (Fig. 9) or in late May when $\tilde{P}$ in the band 4° to 12°S is negative near 0.7 mb (not shown).

5. Relationships between pancake structures and Rossby waves

a. *Eliassen–Palm fluxes*

The left side of Fig. 6 shows Eliassen–Palm (EP) fluxes for cases A, B and C, calculated as described in section 2c. The relatively small size of the heat flux term in $F_{(y)}$ suggests that quasi-geostrophic theory can be used to interpret these fluxes, at least where η is not too different from f. The quasi-geostrophic wave action density for linear waves,

$$A = \frac{1}{2}\bar{q}_y\overline{(\delta y)^2}, \qquad (5.1)$$

is described by

$$\frac{\partial}{\partial t}(\rho_0 A) + (\cos\phi)^{-1}\frac{\partial}{\partial y}(\cos\phi\rho_0 G_y A) + \frac{\partial}{\partial z}(\rho_0 G_z A) = -\alpha\rho_0 A \qquad (5.2)$$

where $\overline{(\delta y)^2}$ is the rms parcel displacement (small for linear waves), $\bar{q}_y$ is the meridional gradient of quasi-geostrophic potential vorticity, and α is a dissipation rate, which we shall assume to be approximately equal to the radiative damping rate. The meridional and zonal components of the Rossby wave group velocity appearing in (5.2) are

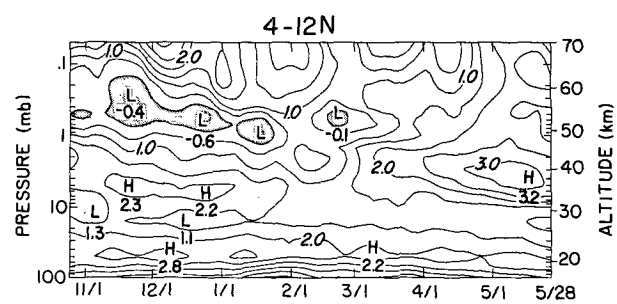

FIG. 9. Time–height section of $\tilde{P}$ (see text section 4) averaged over 4°–12°N. Contour interval 0.5 day^{-1} with negative values shaded. Values have been smoothed ¼–½–¼ in time.

$$G_y = \bar{q}_y \frac{2lk}{K^4} \tag{5.3a}$$

$$G_z = \bar{q}_y \frac{f^2}{N^2} \frac{2mk}{K^4} \tag{5.3b}$$

where k, l, m are wavenumbers in the zonal, meridional and vertical directions, and

$$K^2 = k^2 + l^2 + \frac{f^2}{N^2}\left(m^2 + \frac{1}{4H^2}\right), \tag{5.4}$$

where H is the scale height (cf. Edmon et al., 1980).

For steady, dissipative, linear Rossby waves, (5.2) indicates that the wave action density will decay away from the wave source region with vertical and meridional dissipation length scales $|G_z/\alpha|$ and $|G_y/\alpha|$. For a typical Rossby wave near 30°N, wavelengths are $L_z \sim 50$ km, $L_y \sim 10^4$ km, $L_x \sim 3 \times 10^4$ km, $H \sim 7$ km, $f \sim 7 \times 10^{-5}$ s^{-1}, and $\bar{q}_y \sim 2 \times 10^{-11}$ m^{-1} s^{-1}. Then (5.3) gives $G_y \sim -600$ km (day)$^{-1}$ and $G_z \sim 2$ km (day)$^{-1}$. It would take about two weeks for Rossby wave action to propagate from the winter tropopause to the equatorial mesosphere. The signs of these components are determined by the fact that l and k are of opposite sign, while m and k are of the same sign because of the slopes of Rossby wave phase surfaces in the latitude–longitude and latitude–height planes. For $\alpha^{-1} \sim 3$ days near the stratopause, the horizontal and vertical dissipation length scales are ~2000 km and ~6 km.

For linear quasi-geostrophic Rossby waves, $F_{(y)} \approx \rho_0 G_y A$, and $F_z \approx \rho_0 G_z A$ (except for a constant factor, Edmon et al., 1980). The EP flux vectors displayed in Fig. 6 indicate upward wave action flux from the polar lower stratosphere, refraction toward the equator, and dissipation in the low latitude mesosphere with decay lengths comparable to the dissipation lengths discussed above. The EP flux convergence maxima are located just above the level of the maximum northward incursion of zonal easterlies, very close to the level of the pancake structures, and about 2–3000 km north of the zero wind line in cases A, B and C. In some places, the EP flux penetrates to equatorial latitudes in westerlies, but does not penetrate into the easterlies.

The EP flux vectors split near the large dots shown in Fig. 6, cases A and B, with one branch directed upward, the other equatorward. The pancake structures lie above and equatorward from this split and are associated with strong poleward EP flux near 0.4 mb and 15°N in case B. There is also weak poleward EP flux in the region occupied by pancake structures in case A near 0.5 mb, 10°N, and in case C, near 0.8 mb, 10°N. Because $\eta \leq 0$ in these regions, quasi-geostrophic theory does not apply, and the EP flux cannot be interpreted as wave action flux.

b. *Temporal relationships between pancake structures and Rossby waves*

Figure 10a shows the time–longitude relationship between temperature extrema in pancake structures at 0.4 mb, and those of subtropical Rossby waves at 0.7 mb. Extrema occur at similar longitudes in both signals between approximately 15 and 25 November, 10 and 22 December, and irregularly between about 1 and 12 January. Strong equatorial temperature signatures are not observed when subtropical Rossby waves are weak. Similar statements apply to the wavenumber 1 components of Rossby waves and equatorial temperature anomalies (Fig. 10b).

The situation is more complex with wavenumber 2 (Fig. 10c). When the pancake structures are most intense, the wavenumber 2 component of the temperature field is stationary and intense at 0.4 mb over the equator and at 0.7 mb in the northern subtropics. Between 25 November and 9 December, immediately following the event of case A, wavenumber 2 propagates eastward at 20° longitude (day)$^{-1}$ at the equator and in the northern subtropics. This coherent propagation suggests penetration to the equator of an eastward propagating Rossby wave at that time. Again at the end of the case B event, the equatorial wavenumber 2 component of temperature begins to propagate, but this time, propagation is westward at about 10° longitude per day, and it is not coherent with the strong wavenumber 2 feature in the subtropical lower mesosphere.

The pancake structures have very long zonal scales with wavenumber 1–3 components combining to produce maximum amplitude in certain longitude bands. The coincidence of these events with intense stationary Rossby wavenumber 1 and 2 activity in the subtropical lower mesosphere suggests that the longitudinal structure of the pancake features is selected by the Rossby waves. The absence of pancake structures during late February and May, when inertial instability appears in the 4°–12° latitude band (north of the equator in February and south of the equator in May) but when Rossby waves are weak in the subtropics of both hemispheres, suggests that the Rossby waves may be forcing the observed dynamical response in the tropical mesosphere when inertial stability is weak or negative.

6. Inferences and implications

a. *Relationships to meridional flow and to zonal flow stability*

Figure 11 illustrates several other aspects of the mean flow during case B. The residual mean meridional wind, calculated as described in HL (Fig. 11a) shows a meridional "jet" at 0.4 mb, below the main northward flow of the upper mesosphere. This is associated with an excursion of easterlies into the Northern Hemisphere at the same level (Fig. 6B). The mean meridional

flow can advect easterlies across the equator only where $\bar{\eta} < 0$, i.e., only in a region of zonal mean inertial instability. Convergence of EP flux also contributes to weakening of the westerlies, and an exceptionally strong center of EP flux convergence near 30°N and 0.3 mb may be playing that role (Fig. 6B, left). This convergence may be enhanced at that location and time because of the mean meridional circulation whose magnitude (~ 3 m s^{-1}) is significant compared to the Rossby wave group velocity (~ -6 m s^{-1}) estimated for that region. Since it opposes the group velocity, it would act to decrease the meridional dissipation length of Rossby waves and enhance the EP flux convergence in the region in the manner proposed by Schneider and Watterson (1984). In the inertially stable region, north of about 25°N, quasi-geostrophic theory is qualitatively correct and it states that strong northward meridional flow will tend to balance EP flux convergence (Eq. 2.6). Thus, there is evidence for a complex set of links between inertial instability, pancake structures, mean meridional flow, and Rossby wave EP flux convergence.

Instability may be a cause of the pancake features, and inflection line instability should be considered as a possibility. Figure 11b shows that there are several regions where $\beta - \bar{u}_{yy} < 0$, so that inflection line instability of barotropic type might occur. However, unlike the pancake structures, unstable waves of this type should propagate phase in both latitude and longitude and should have a large vertical scale (Pfister, 1985). One or more unstable modes having these characteristics were observed to be associated with the strongly unstable region near 25°S and 0.1 mb in Fig. 11b (Burks and Leovy, 1986), but the pancake structures are very different.

Evidence relating pancake structures to a broad inertially unstable band in the equatorial mesosphere was presented in section 4. Thus inertial instability, or at least enhanced response to forcing in an inertially weak region, is preferred. Figure 11c shows that, in addition to the band of strong inertial instability in the lower mesosphere between 0° and 12°N during case B, there is a band of weak inertial stability near 0.3 mb connecting this band to a region of still weaker or negative stability near 0.3 mb, 20°N. Since f is larger here and $\partial^2\delta_y/\partial t^2 = -f\tilde{P}\delta_y$, this second region may be significant for inertial acceleration. The pancake structures center in the latitude-height region of weakest stability, and extend poleward to about 20–25°N (Figs. 3, 4, 5). Thus we infer that their meridional scale is controlled by the width of the region of weak or negative inertial stability. Next we consider the factors controlling their vertical scale.

b. *Vertical scale*

Zonally asymmetric meridional circulations in the presence of strong cross-equatorial shear have been diagnosed in a numerical model (Hunt, 1981). Hunt's circulation cells were apparently due to inertial instability. They were smaller than the cells we observe meridionally as well as vertically.

The theory of low wavenumber inertial instability has been developed by Boyd and Christidis (1982) and Dunkerton (1983). Boyd and Christidis found that growth rates were larger for zonally asymmetric than for zonally symmetric perturbations. In the symmetric case, Dunkerton (1981) assumed an eddy diffusivity, ν, which led to a marginally stable value of meridional shear, Γ_c, and a finite vertical scale, L_z. Using a Hermite spectral model to analyze the asymmetric case, he found that the marginally stable shear is approximately 26% less than in the symmetric case. Taking $N = 0.02$ s^{-1} and $\beta = 2.3 \times 10^{-11}$ m^{-1} s^{-1} in his equation (3.9), for ν in units of m^2 s^{-1} and Γ_c in day^{-1},

$$\Gamma_c \approx 1.9\nu^{1/5}. \tag{6.1}$$

Substituting (6.1) into his equation (2.3) gives an expression for the dependence on threshold shear of vertical wavelength L_z (in kilometers) for the fastest growing mode:

$$L_z \approx 0.67\Gamma_c^2. \tag{6.2}$$

For sufficiently large shear ($\Gamma > \Gamma_c$), a spectrum of inertial circulations will grow, dominated by the vertical scale (6.2). For $\Gamma < \Gamma_c$ dissipation will suppress all modes.

At a particular longitude, meridional overturning is expected to occur in a stack of cells, with temperature perturbations maximizing over the equator and over the latitude where $\Gamma = f$ (Dunkerton, 1981; 1983). In these cells, $u'v'$ is expected to be equatorward consistent with wave growth and a tendency to reduce Γ and restore a stable profile of angular momentum. The preferred zonal wavenumber is in the range

$$0 < k^* < 12.6/\Gamma_c, \tag{6.3}$$

where $k^* = ka$ is nondimensional and Γ_c is in day^{-1}, but spectral selection in this range is weak. Inertial waves are generally expected to have nonzero zonal phase speeds (Boyd and Christidis, 1982; Dunkerton, 1983).

Table 1 contains values of ν which stabilize integer values of Γ (6.1), together with the corresponding preferred vertical length scale (6.2) and cutoff zonal wavenumber (6.3). Gravity waves breaking in the lower mesosphere may cause $\nu \sim 100$ m^2 s^{-1} (Lindzen, 1981). This value corresponds to $\Gamma_c \sim 4.5$ day^{-1}, $L_z \sim 13$ km, and $k^* \leq 2$. Pancake structures typically have $L_z \sim 14$ km (Fig. 2), project primarily onto waves 1 and 2 (Fig. 7), and occur when cross equatorial shears are $\sim$4–6 day^{-1} (Fig. 2c of HL).

Agreement between observations, the predicted structure, and the predicted parameters of Table 1 is good for $\nu \sim 100$ m^2 s^{-1}, but the theory does not yet

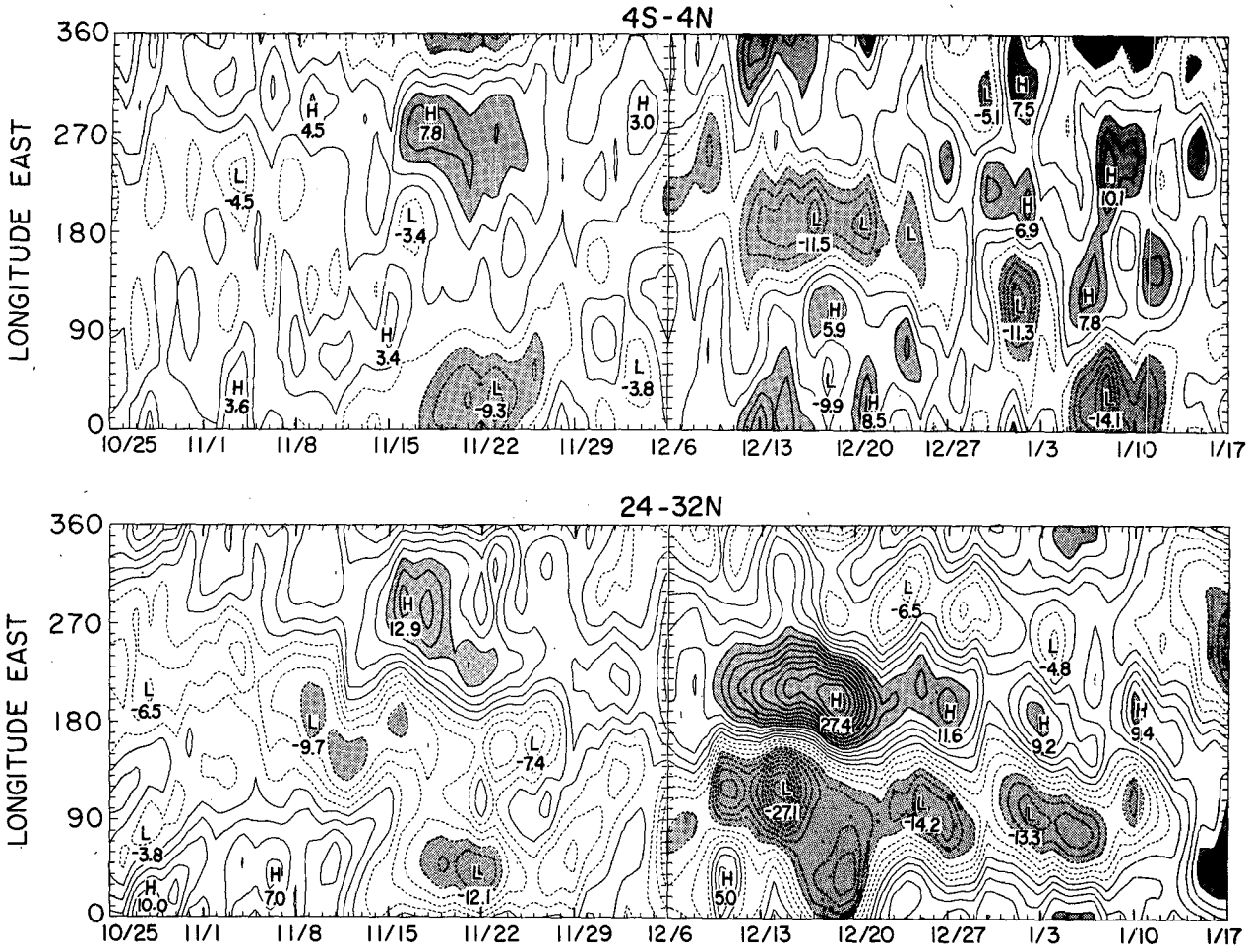

FIG. 10a. Longitude–time sections of LIMS temperature waves 1–3 for the period 25 October 1978–17 January 1979, averaged over 4°S–4°N at 0.4 mb (upper) and over 24–32°N at 0.7 mb (lower). The contour interval is 2 K. Values larger than ±4 K (upper) and ±8 K (lower) are shaded.

account for several observed aspects of the pancake structures.

1) Inertial waves are expected whenever Γ is large. Yet pancake structures wax and wane with adjacent Rossby wave activity, while $\tilde{P}$ remains about the same.

2) In a zonally symmetric barotropic basic state the theory gives no means of selecting and maintaining a particular vertical location or longitudinal phase for a circulation cell. Pancake structures maintain a particular vertical and zonal phase for many days at a time.

3) Inertial waves predicted by the theory would migrate zonally with respect to the mean flow in which they arise. Since the pancake structures reside in flow which varies considerably in space and time, it is difficult to account for their observed quasi-stationarity on the basis of inertial instability theory alone.

TABLE 1. Parameters for the theory of eddy diffusivity-selected inertial waves.

Eddy diffusivity ν ($m^2 s^{-1}$)	Critical shear Γ_c (day^{-1})	Vertical wavelength L_z (km)	Cutoff zonal wavenumber k^*
0.04	1	0.7	12
1.3	2	2.7	6
9.8	3	6.0	4
41.0	4	11.0	3
130.0	5	17.0	2
310.0	6	24.0	2
680.0	7	33.0	1

Since inertial instability is a parcel instability, local conditions should determine parcel acceleration. It is likely that the zonal scale and phase of adjacent subtropical perturbations determines the longitudinal distribution of inertial circulations.

In inertial instability theory inertial waves are assumed to be free modes and the values of ω and k for maximum growth rate are sought (Dunkerton, 1981; Boyd and Christidis, 1982; Dunkerton, 1983). Instead, we suppose here that ω and k are determined by forcing (Rossby waves) and seek a vertical scale. For small k

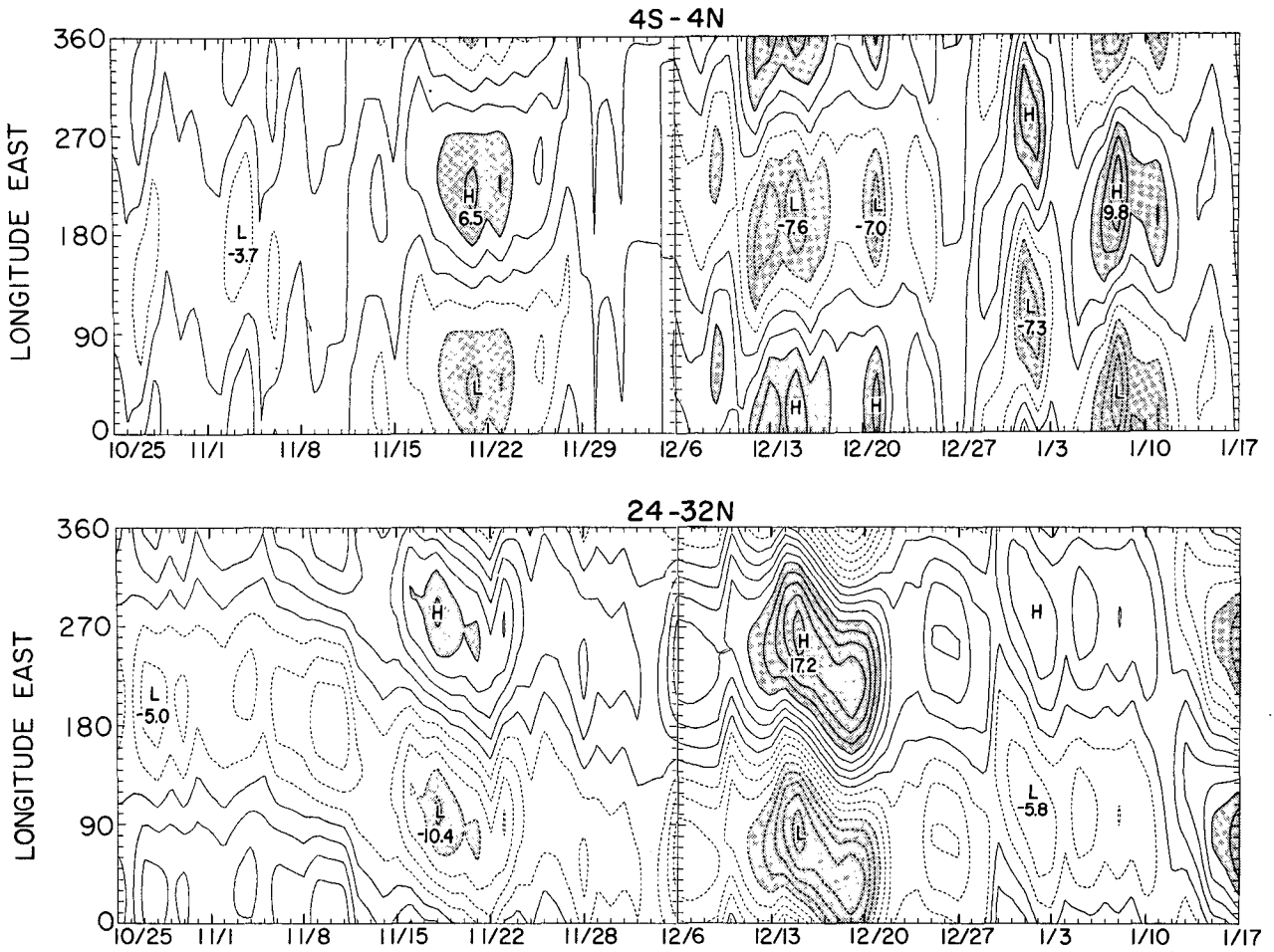

FIG. 10b. As in Fig. 10a, except for wave one only.

Laplace's tidal equation on a sheared equatorial β-plane has solutions for

$$\frac{m}{N\beta}(\omega^2+\Gamma^2/4)=2n+1, \quad n=0,1,2,\cdots \tag{6.4}$$

where n is the latitudinal mode number (e.g., Holton, 1975, pp. 64–65; Boyd, 1978; Dunkerton, 1981). For the Rossby wave forced solution, $\omega \sim 0$, and the gravest latitudinal mode will have the vertical scale

$$L_z=\frac{\pi}{2N\beta}\Gamma^2. \tag{6.5}$$

This result is very similar to (6.2), except here a dominant vertical scale is obtained by constraining the frequency, rather than by the dissipation of smaller-scale modes. Since $y = 0$ and $y = \Gamma/\beta$ bound the region of inertial instability, a meridional wavelength for circulations is $L_y = 2\Gamma/\beta$. Equation (6.5) may be rewritten

$$L_z=\frac{\pi}{4}\frac{|\Gamma|}{N}L_y. \tag{6.6}$$

The vertical separation between temperature anomalies of opposite sign, $L_z/2$, will be large where vertical stability is small, where cross-equatorial shear is large, and where the meridional breadth of the inertially unstable region is large.

Both Dunkerton's theory of viscous inertial instability and the foregoing consideration of the vertical scale of a forced stationary equatorial disturbance ignore vertical shear, $\bar{u}_z$. The measure of the importance of vertical shear is the inverse Richardson number, Ri^{-1}. Stone (1966) showed that inviscid inertially unstable waves would arise in a flow in which $\frac{1}{4} < |\mathrm{Ri}| < 1$, even where $\eta > 0$. In the equatorial mesosphere, the mean value of Ri is typically about 30, but there are strong variations with longitude arising out of large planetary scale zonal variations.

Figure 12 illustrates how large zonal wind variations can be between Ft. Sherman (9.3°N, 80.0°W) and Kwajalein (8.7°N, 167.7°W). These wind differences, which can be compared with the balance winds in Fig. 5, arise partly from the pancake structures themselves, and partly from longer-lived longitudinal variations due to Rossby waves extending into the subtropics. As a further illustration, zonal winds near 180°E in Fig. 13 are compared with zonal mean winds in Fig. 6B. The marked differences show that longitudinally local values of $\bar{u}_y$ and Ri can depart significantly from their zonal mean values. For example, near 0.4 mb the me-

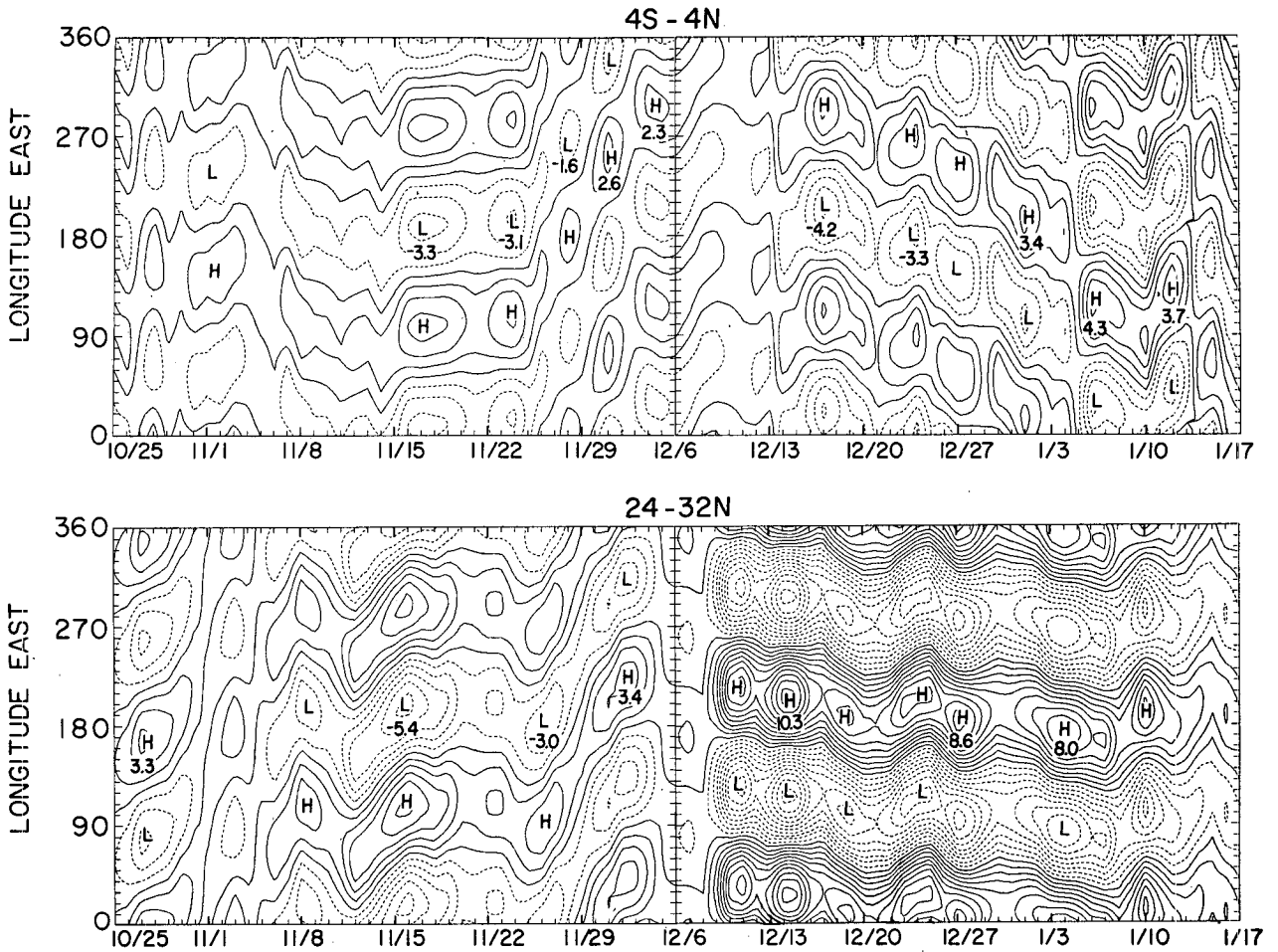

FIG. 10c. As in Fig. 10b, except for wave two only. The contour interval is 1 K, and shading is omitted.

ridional shear between 16°N and 24°N for the zonal mean and 180°E are 4.4 (day)$^{-1}$ and 5.3 day^{-1}, respectively, while f at 20°N is 4.3 (day)$^{-1}$. Zonal mean and local values of $\tilde{P}$ are -0.1 day^{-1} and -1.0 day^{-1}. Near 4°N zonal mean and local Richardson numbers in the layer 0.4–0.7 mb are ~30 and 1.5, respectively. Rossby waves and pancake structures together induce long-lasting zonal asymmetries in background flow structure, particularly in $\bar{u}_y$ and Ri, as well as in meridional parcel displacements.

We are not aware of a complete theory of inertial instability that allows for longitudinally varying meridional and vertical shear, but the fact that inertial instability is a parcel instability makes it appropriate to address the role of Ri with a simple energy argument. In an inertially unstable region ($\tilde{P} < 0$), meridionally displaced parcels will accelerate throughout the width $L_y/2$ of the unstable zone, with horizontal convergence or divergence and vertical motion occurring at the boundaries. Growth or maintenance of a meridional circulation cell will be possible only if the net work per unit mass done on each parcel traveling through its vertical and meridional branches is positive. Since isentropic surfaces are nearly horizontal, acceleration in the branch $(0, L_z/2)$ is $-N^2\delta z$ and in the branch $(0, L_y/2)$ is $-f[f(1 - 1/\mathrm{Ri}) - u_y]\delta y$, and the work criterion becomes

$$-\int_0^{L_z/2} N^2 z dz - \int_0^{L_y/2} f[f(1-1/\mathrm{Ri}) - u_y] y dy > 0. \quad (6.7)$$

Assuming $\bar{u}_y = \Gamma$ and $f = \beta y$, evaluating the integrals, then substituting $L_y = 2\Gamma/\beta$, (6.7) becomes

$$L_z < L_y \frac{|\Gamma|}{N}\left(\frac{4 - 3(1 - 1/\mathrm{Ri})}{6}\right)^{1/2}. \quad (6.8)$$

This reduces to

$$L_z < \frac{0.4|\Gamma|}{N} L_y \approx \frac{0.8}{N\beta}\Gamma^2 \quad \text{for} \quad \mathrm{Ri} \to \infty, \quad (6.9a)$$

$$L_z < \frac{0.8|\Gamma|}{N} L_y \approx \frac{1.6}{N\beta}\Gamma^2 \quad \text{for} \quad \mathrm{Ri} \approx 1. \quad (6.9b)$$

Thus all three approaches give quite similar results. With $N \approx 0.017$ s^{-1}, and $\Gamma = 5$ (day)$^{-1}$, (6.9) gives $\delta > 370$ which is in agreement with observational estimates. Given the meridional scale $L_y \sim 2\Gamma/\beta$, determined by the width of the inertially unstable region, the vertical scale is then determined by energetic requirements of the motion, and is not much influenced

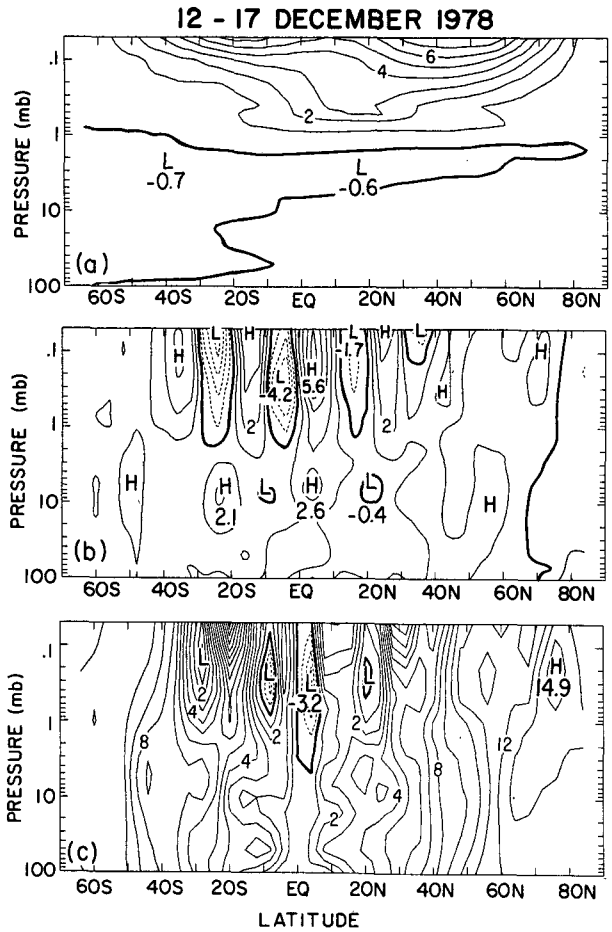

FIG. 11. Latitude–height sections of six day average (a) residual mean meridional wind, contour interval 1 m s^{-1}, (b) $\beta - \bar{u}_{yy}$ normalized by $2\Omega/a$, contour interval 1, and (c) $\tilde{P}$ (see text) contour interval 1 day^{-1}, for the period 12–17 December 1978; $\bar{u}_y$ was smoothed ¼–½–¼ in latitude, then $\bar{u}_{yy}$ was smoothed twice again in calculating $\tilde{P}$ and $\beta - \bar{u}_{yy}$.

by Ri variations over a large range. The meridional scale may be determined by the effective viscosity through (6.1) if the inertial motions are marginally unstable, or by large scale circulation processes controlling the structure of the winter hemisphere westerlies.

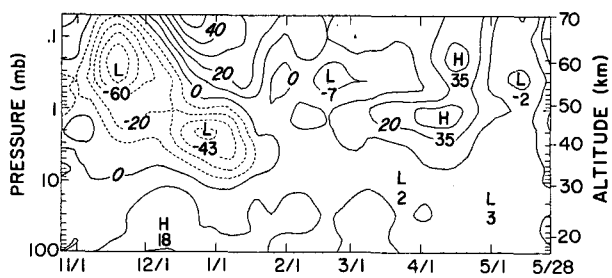

FIG. 12. Time–height section of LIMS balance zonal winds at Fort Sherman (9.3°N, 80.0°W) minus those of Kwajalein (8.7°N, 167.7°E). The contour interval is 10 m s^{-1}. Values have been smoothed ¼–½–¼ in time.

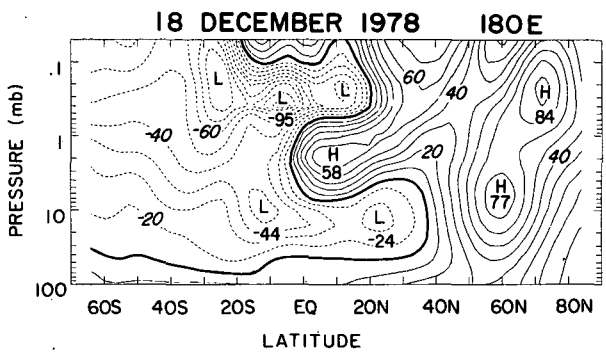

FIG. 13. Latitude–height sections of LIMS balance winds at 180°E for case B. The contour interval is 10 m s^{-1}. Waves 0–3 are included in the analysis. Values have been smoothed ¼–½–¼ in latitude.

Rossby waves appear to provide forcing at the subtropical boundaries which fixes the locations of the observed large scale equatorial structures.

c. *Feedback effects on the mean flow*

Pancake structures tend to transport westerly zonal momentum toward the equator across the domain $L_y/2$ in which they are active. This implies convergence of westerly momentum flux at the southern boundary of their domain and divergence at the northern boundary. As a result they tend to suppress the cross-equatorward transport of easterlies, confine the strong winter westerlies poleward of the subtropics, inertially stabilize the meridional shear of the zonal wind, and produce a broad tropical region of weak zonal mean winds such as that shown in Fig. 5. This pattern of zonal wind driving can be seen in Fig. 6B, where EP flux divergence is producing strong zonal wind accelerations near 10°N, 0.3 mb, and strong decelerations to the north near 30°N, 0.3 mb. The magnitude of the accelerations, several m s^{-1} (day)$^{-1}$ or more, can easily be adequate to balance the accelerations produced by the mean meridional flow shown in Fig. 11a.

The pancake structures also transport momentum vertically. Consider the warm–cold pairs depicted schematically in Fig. 8a. Because the cells approximately satisfy the long-wave approximation, $u' \sim \Phi'$. Where cold air underlies warm air $\Phi' < 0$ between the temperature extrema, and eddy vertical motion transports easterly momentum toward the axis of maximum eddy meridional flow from above and below. Where warm air underlies cold air, the eddy vertical motion transports zonal momentum away from this axis, so that $\overline{u'w'} > 0$ above the axis, and $\overline{u'w'} < 0$ below the axis for either configuration. This pattern of momentum flux and the corresponding pattern of convergence is shown schematically in Fig. 8b. For vertical velocity and zonal eddy velocity amplitudes of 0.5 cm s^{-1} and 20 m s^{-1}, and $L_z \sim 14$ km, the resulting mean zonal flow acceleration can exceed 1 m s^{-1} day^{-1}. Thus these vertical fluxes can play an important, though probably secondary, role in modifying the mean zonal wind.

Their effect is to enhance zonal mean easterlies along the axis between overlying cells for either sign of eddy meridional wind, and at the same time to vertically shrink the region of easterlies. In this way, they may help account for the shallow depth of the incursion of mesospheric easterlies into the winter hemispheres shown on the right side of Figs. 6B, C.

Pancake structures can redistribute zonal mean flow momentum in their region of activity, but they cannot change the mean angular momentum of that region.

7. Concluding remarks

We have identified a class of equatorial zonally asymmetric nonpropagating thermal disturbance in the lower mesosphere. The disturbances, consisting of two or three vertically stacked temperature extrema are confined to regions and times where the zonal mean inertial stability is very weak or negative over a broad band from the equator to about 20° latitude in the winter hemisphere. Their vertical scale is controlled by the relation $L_z \sim (\Gamma/N)\, L_y$. Consequently, they might occur when the width of the inertially unstable region, L_y, is much smaller, but would be below the vertical resolution limit of LIMS at such times. However, even when there is a broad inertially weak or unstable band, they are observed only when forcing of the lower tropical mesosphere by wavenumber one and two Rossby waves is strong, and we infer that their occurrence and longitude structure is conditioned by the Rossby waves.

These structures can have an important influence on the zonal mean flow in the tropical mesosphere, and so should be taken into account in future models of this region. The LIMS dataset permits a detailed analysis of them only during the 1978/79 winter. However, since their signature can be identified in low-latitude rocketsonde data, it should be possible to derive some information about their interannual variability. It is likely that these structures contribute to the large wind variances which Hopkins (1975) observed in the descending easterlies of the SAO.

Acknowledgments. We wish to thank Peter Haynes, John Boyd, Tim Dunkerton, Kevin Hamilton, and Walter Robinson for stimulating conversations. Hiroshi Kanzawa and an anonymous reviewer made valuable suggestions. This work is based in part on MHH's Ph.D. dissertation at the University of Washington. The first two authors were supported by NASA under Grant NAGW-471. The National Center for Atmospheric Research is sponsored by the National Science Foundation.

REFERENCES

Andrews, D. G., and M. E. McIntyre, 1976: Planetary waves in horizontal and vertical shear: The generalized Eliassen-Palm relation and mean zonal acceleration. *J. Atmos. Sci.*, **33**, 2031–2048.

Bailey, P. L., and J. C. Gille, 1986: Inversion of LIMS radiance measurements: an operational algorithm. *J. Geophys. Res.*, **19**, 2757–2774.

Boyd, J. P., 1976: The noninteraction of waves with the zonally-averaged flow on a spherical earth and the interrelationships of the eddy fluxes of energy, heat and momentum. *J. Atmos. Sci.*, **33**, 2285–2291.

——, 1978: The effects of latitudinal shear on equatorial waves. Part I: Theory and methods. *J. Atmos. Sci.*, **35**, 2236–2258.

——, and Z. D. Christidis, 1982: Low wavenumber instability on the equatorial beta-plane. *Geophys. Res. Lett.*, **9**, 769–772.

Burks, D., and C. Leovy, 1986: Planetary waves near the mesospheric easterly jet. *Geophys. Res. Lett.*, **13**, 193–196.

Coy, L., and M. H. Hitchman, 1984: Kelvin wave packets and flow acceleration: A comparison of modeling and observations. *J. Atmos. Sci.*, **41**, 1875–1880.

Dunkerton, T. J., 1981: On the inertial instability of the equatorial middle atmosphere. *J. Atmos. Sci.*, **38**, 2354–2364.

——, 1983: A nonsymmetric equatorial inertial instability. *J. Atmos. Sci.*, **40**, 807–813.

Edmon, H. J., B. J. Hoskins and M. E. McIntyre, 1980: Eliassen-Palm cross sections for the troposphere. *J. Atmos. Sci.*, **37**, 2600–2616.

Eliassen, A., and E. Kleinschmidt, 1957: Dynamic Meteorology. In *Handbuch der Physik*, Vol. 48, Springer-Verlag, 1–154.

Fels, S., 1982: A parameterization of scale-dependent radiative damping rates in the middle atmosphere. *J. Atmos. Sci.*, **39**, 1141–1152.

——, 1984: The radiative damping of short vertical scale waves in the mesosphere. *J. Atmos. Sci.*, **141**, 1755–1764.

Gille, J. C., and J. M. Russell III, 1984: The Limb Infrared Monitor of the Stratosphere (LIMS) experiment description, performance, and results. *J. Geophys. Res.*, **89**, D4, 5125–5140.

——, ——, P. L. Bailey, L. L. Gordley, E. E. Remsberg, J. H. Leinesch, W. G. Planet, F. B. House, L. V. Lyjak and S. A. Beck, 1984: Validation of temperature retrievals obtained by the Limb Infrared Monitor of the Stratosphere (LIMS) experiment on Nimbus 7. *J. Geophys. Res.*, **89**, D4, 5147–5160.

Hitchman, M. H., and C. B. Leovy, 1986: Evolution of the zonal mean state in the equatorial middle atmosphere during October 1978–May 1979. *J. Atmos. Sci.*, **43**, 3159–3176.

Holton, J. R., 1975: *The Dynamic Meteorology of the Stratosphere and Mesosphere. Meteor. Monogr.* No. 37, Amer. Meteor. Soc., 216 pp.

Hopkins, R., 1975: Evidence of polar-tropical coupling in upper stratospheric zonal wind anomalies. *J. Atmos. Sci.*, **32**, 712–719.

Hunt, B. G., 1981: The maintenance of the zonal mean state of the upper atmosphere as represented in a three-dimensional general circulation model extending to 100 km. *J. Atmos. Sci.*, **38**, 2172–2186.

Krishnamurti, T. N., and V. Wong, 1979: A simulation of cross-equatorial flow over the Arabian Sea. *J. Atmos. Sci.*, **36**, 1895–1907.

Lindzen, R. S., 1981: Turbulence and stress owing to gravity waves and tidal breakdown. *J. Geophys. Res.*, **86** (C10), 9707–9714.

Pfister, L., 1985: Baroclinic instability of easterly jets with application to the summer mesosphere. *J. Atmos. Sci.*, **42**, 313–330.

Reverdin, G., and G. Sommeria, 1983: The dynamical structure of the planetary boundary layer over the Arabian Sea, as deduced from constant-level balloon trajectories. *J. Atmos. Sci.*, **40**, 1435–1452.

Robinson, W. A., 1986: Application of the quasigeostrophic Eliassen-Palm flux to the analysis of stratospheric data. *J. Atmos. Sci.*, **43**, 1017–1023.

Salby, M. L., D. L. Hartmann, P. L. Bailey and J. C. Gille, 1984: Evidence for equatorial Kelvin modes in Nimbus 7 LIMS. *J. Atmos. Sci.*, **40**, 220–235.

Schneider, E. K., and I. G. Watterson, 1984: Stationary Rossby wave propagation through easterly layers. *J. Atmos. Sci.*, **41**, 2069–2083.

Shuman, F. G., 1957: Numerical methods in weather prediction: I. The balance equation. *Mon. Wea. Rev.*, **85**, 329–332.

Stone, P. H., 1966: On non-geostrophic baroclinic stability. *J. Atmos. Sci.*, **23**, 390–400.

Stout, J. E., and J. A. Young, 1983: Low-level monsoon dynamics derived from satellite winds. *Mon. Wea. Rev.*, **111**, 774–798.

van Tuyl, A. H., 1986: Advective influences on forced tropical motions. *J. Atmos. Sci.*, **43**, 141–161.